The understanding of electronic excitations of C_{60} on graphite

2004 J. Phys.: Condens. Matter 16 6257

(http://iopscience.iop.org/0953-8984/16/34/023)

INSTITUTE OF PHYSICS PUBLISHING JOURNAL OF PHYSICS: CONDENSED MATTER

J. Phys.: Condens. Matter **16** (2004) 6257–6265 PII: S0953-8984(04)81697-7

The understanding of electronic excitations of C_{60} on graphite

M F Luo[1,2], Z Y Li[3,4] and W Allison[1]

[1] Cavendish Laboratory, Cambridge University, Madingley Road, Cambridge CB3 0HE, UK
[2] Department of Physics, National Central University, No 300, Jungda Road, Jungli, 32054, Taiwan
[3] Nanoscale Physics Research Laboratory, School of Physics and Astronomy, University of Birmingham, Birmingham B15 2TT, UK

E-mail: ziyouli@nprl.ph.bham.ac.uk

Received 30 May 2004
Published 13 August 2004
Online at stacks.iop.org/JPhysCM/16/6257
doi:10.1088/0953-8984/16/34/023

Abstract

Electron energy loss spectroscopy has been used to probe the coverage-dependent electronic excitations from a C_{60} covered graphite surface. In the energy region corresponding to the optical band-gap of the bulk C_{60} solid, the dipole-scattering contribution to the loss features is simulated by a double dielectric layer model. We find that a good agreement between the simulated spectra and the experimental results can be achieved for a C_{60} multilayer. However, an additional energy loss channel is required in order to describe the electronic excitations for a C_{60} monolayer. The possible significances of this finding are discussed.

1. Introduction

Since the discovery of C_{60} over a decade ago, various techniques have been used to study the adsorption of this molecule on substrate surfaces. The ultimate goal is twofold:

(1) to have a good control of the growth of C_{60} thin films in order to make use of the unique properties of this system in potential applications, and
(2) to have a better understanding of the underlying physics in this system.

Adsorption of C_{60} on graphite substrate has become a model system to study the C_{60}–substrate interaction [1–12]. Electron energy loss spectroscopy (EELS) has been used to understand, among other properties, the C_{60} thin film growth mode [5–7]. EELS can also reveal a rich physics of C_{60} thin films. For example, in the electronic excitation regime, one finds not only the dipole-forbidden transition between the highest occupied molecular orbital (HOMO) to lowest

[4] Author to whom any correspondence should be addressed.

unoccupied molecular orbital (LUMO), but also the spin-forbidden triplet excitation [13, 14]. The coverage dependence of these excitations is of particular interest for their potential role in revealing the interfacial electronic structure. We discovered that the excitation strength of the dipole-forbidden HOMO–LUMO transition is quenched at submonolayer coverage [5, 7]. In the present work, we investigate the C_{60} coverage dependence of the dipole-allowed transition in the C_{60}–graphite system. By employing a double dielectric layer model, we found that a good agreement between the simulation and the experimental EELS spectra can be obtained for a C_{60} multilayer. The same analysis can be extended to a C_{60} monolayer if the effective dielectric function for (sub)monolayer coverage has an imaginary component, even in the optical gap region of the bulk of C_{60}.

2. Coverage dependence of impact excitation spectroscopy

The experimental details have been described in one of our previous publications [5]. Briefly, the sample used is a highly oriented pyrolytic graphite (HOPG). Depositions of C_{60} (99.95% purity) were made while the substrate was at room temperature. The EELS spectra were taken with an incident electron beam energy of 12 eV and at the specular scattering geometry. Figure 1(a) shows the experimental result for the energy range corresponding to the 'optical gap' of the bulk C_{60}. Qualitatively, the spectral features can be identified as an intraband excitation continuum arising from the semi-metallic graphite substrate superimposed by a dipole-forbidden C_{60} HOMO–LUMO transition [13, 15]. Since the latter is not observed in the dielectric response of the bulk materials, which is dominated by the dipole process, we have treated the C_{60} contribution to the loss features by impact scattering in our previous work on the growth of C_{60} thin films on graphite [5]. We have parameterized the spectra in terms of a linear combination of two reference EELS spectra, corresponding to the bare graphite and the thickest C_{60} films examined respectively [5, 7]. The fitting range was from 1 to 2.5 eV. The solid curve in figure 1(a) shows an example of such fitting for a C_{60} deposition time of 210 s. From the fitting, we obtained two weighting parameters, ξ_g and $\xi_{C_{60}}$, as a function of C_{60} coverage. Both ξ_g and $\xi_{C_{60}}$ can be used as a measure of the strength of scattering from the substrate and the C_{60} film respectively. They should contain information about both the thickness dependence of the electronic excitations as well as the morphology of the C_{60} overlayer. We found an unusually small $\xi_{C_{60}}$ for very low C_{60} coverage, suggesting that the HOMO–LUMO transition of the first C_{60} layer is suppressed at specular electron scattering geometry, possibly due to a substrate-induced quenching effect [7]. Because the impact scattering is a short-range interaction, we have assumed that its excitation probability is directly proportional to the number of C_{60} molecules present at the topmost layer. In our previous publication [5], we have employed a one-parameter growth model for C_{60}, with the key parameter describing the probability for a C_{60} molecule descending to the preceding layer. Figure 1(b) displays the fitting result. Here we extend the investigation to the C_{60} coverage dependence of ξ_g.

3. Two-layer dielectric model

To simulate the behaviour of ξ_g, i.e., the coverage dependence of the substrate response at the C_{60}–graphite interface, we have treated the system by employing a two-layer dielectric model. In this model, the C_{60} overlayer behaves like a uniform dielectric, and the reflection coefficient for incident electrons is assumed to be constant. The electron scattering cross section from such a dielectric system is described by an effective dielectric function, which depends on the dielectric functions of the substrate and that of the overlayer as well as the thickness of

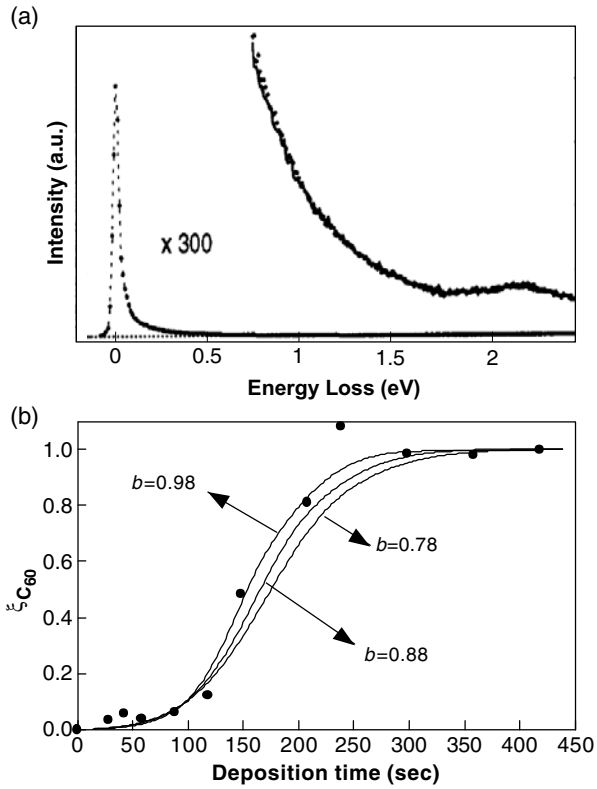

Figure 1. (a) Electron energy loss spectrum from 210 s. Deposition of C_{60} on graphite at room temperature. The incident beam energy is 12 eV. The incident and detected angles are 60°. (b) Measured and simulated variation of the impact scattering from a C_{60} overlayer during growth. (●) Experimental data, while the curves are fitted results using different values of the step-crossing parameter b, as indicated. The figure is reproduced from [7].

the overlayer [16]. To account for the surface roughness, we have assumed that the total cross section function of the C_{60}–graphite system can be written as a summation over the bare graphite surface region and various C_{60}-covered regions as follows:

$$\alpha_{\text{total}}(\Delta E, t) = \sum_{i=0} (\theta_i(t) - \theta_{i+1}(t))\alpha_i(\Delta E), \tag{1}$$

in which θ_i is the coverage of the ith C_{60} overlayer, and $\alpha_i(\Delta E)$ is the cross section function for inelastic scattering over the area covered by i C_{60} overlayers. $\theta_i(t)$ is determined by a growth model characterized by a probability of a molecule crossing a descending step [5]. For dipole scattering, we have the cross section (see [16])

$$\alpha_i(\Delta E) = \frac{\mathrm{d}^2 S}{\mathrm{d}\Omega(\hat{k})\,\mathrm{d}w} \propto k_z^2 \left(\frac{k}{k^{(I)}}\right) \frac{1}{Q_\parallel} \Phi(Q_\parallel, k_z)[n(w)+1]\,\mathrm{Im}\left[\frac{-1}{1+\tilde{\varepsilon}(Q_\parallel, w)}\right], \tag{2}$$

in which the Bose factor, $n(w) = \frac{1}{\exp(\hbar w/k_{\mathrm{B}}T)-1}$, is close to zero at room temperature. The $\Phi(Q_\parallel, k_z)$ can be approximated by the expression

$$\approx \frac{4|R|^2 Q_\parallel^2}{[Q_\parallel^2 + (k_z - k_z^{(I)})^2]^2}, \tag{3}$$

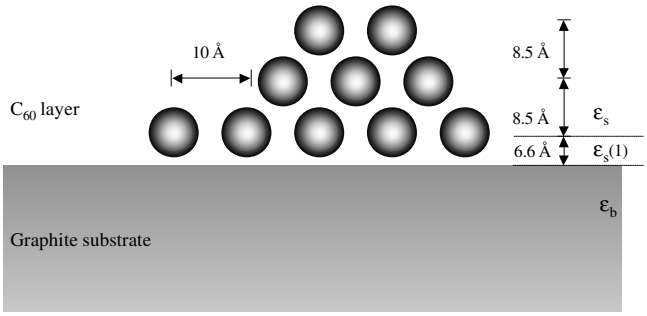

Figure 2. A schematic drawing of a C_{60} overlayer on graphite as assumed in the calculation of the effective dielectric function of C_{60}-covered graphite.

in which k_z and $k_z^{(I)}$ are the components of the wavevector perpendicular to the surface for the scattered electrons and the incident electrons respectively, $Q_\parallel = k_\parallel^{(I)} - k_\parallel$ is the component of the momentum transfer wavevector parallel to the surface, and R ($=R_{C_{60}}$ for $\alpha_{\neq 0}$ and $=R_g$ for α_0) is the surface reflection coefficient. In this cross section function, the loss function $\mathrm{Im}\left[\frac{-1}{1+\tilde{\varepsilon}(Q_\parallel, w)}\right]$ or the effective dielectric function $\tilde{\varepsilon}(Q_\parallel, w)$ is the key material-specific parameter governing the scattering cross section. The effective dielectric function for a two-layered system is given by

$$\tilde{\varepsilon}(Q_\parallel, w) = \varepsilon_s(w)\left[\frac{1 + \Delta(w)\exp(-2Q_\parallel d)}{1 - \Delta(w)\exp(-2Q_\parallel d)}\right], \tag{4}$$

with

$$\Delta(w) = \frac{\varepsilon_b(w) - \varepsilon_s(w)}{\varepsilon_b(w) + \varepsilon_s(w)}, \tag{5}$$

where ε_b and ε_s denote the dielectric function of the substrate and the surface layers respectively, and d is the thickness of the surface layers [16]. The wavevector dependence of ε_b and ε_s was ignored, as $Q_\parallel$ is small in our case (of the order of 0.065–0.09 Å^{-1}). The schematics of the two-layered model is shown in figure 2. The value of ε_b for the graphite substrate used in the simulation is obtained from Danels *et al* [17]. The C_{60} layers above the first layer are treated as those in a thick C_{60} film. Values of ε_s derived from optical and EELS experiments on thick C_{60} films are thus employed [18]. In the energy loss range of interest, 1–2.5 eV, $\varepsilon_s \approx 3.61$. To account for possible interfacial effects, we have represented the dielectric function of the first C_{60} overlayer, $\varepsilon_s(1)$, as an adjustable parameter. The thickness of the first C_{60} is assumed to be 6.6 Å and the interlayer distance for the subsequent layers as 8.5 Å [19].

The key point of our simulation is to derive an effective dielectric function for the two-layer system by an iterative application of equation (4). To account for the possible difference between the dielectric response of the first and subsequent C_{60} layer, we first treat the two-layer system consisting of graphite and the first C_{60} monolayer as a new substrate with an effective dielectric function. Then, the additional C_{60} overlayer is considered as an overlayer in a new effective two-layer system. In this way, we obtained the effective dielectric functions for the areas covered by C_{60} films of various thicknesses. The two-layer dielectric model has been successfully applied to the studies of surface optical constants, and surface electronic states of silicon and germanium [20], as well as to the surface roughness of a dielectric overlayer on substrates [21]. Our simulation was done at a representative energy loss point, 1 eV. The validity of the approach will be demonstrated with the good fit using reconstructed EELS spectra to the original EELS spectra.

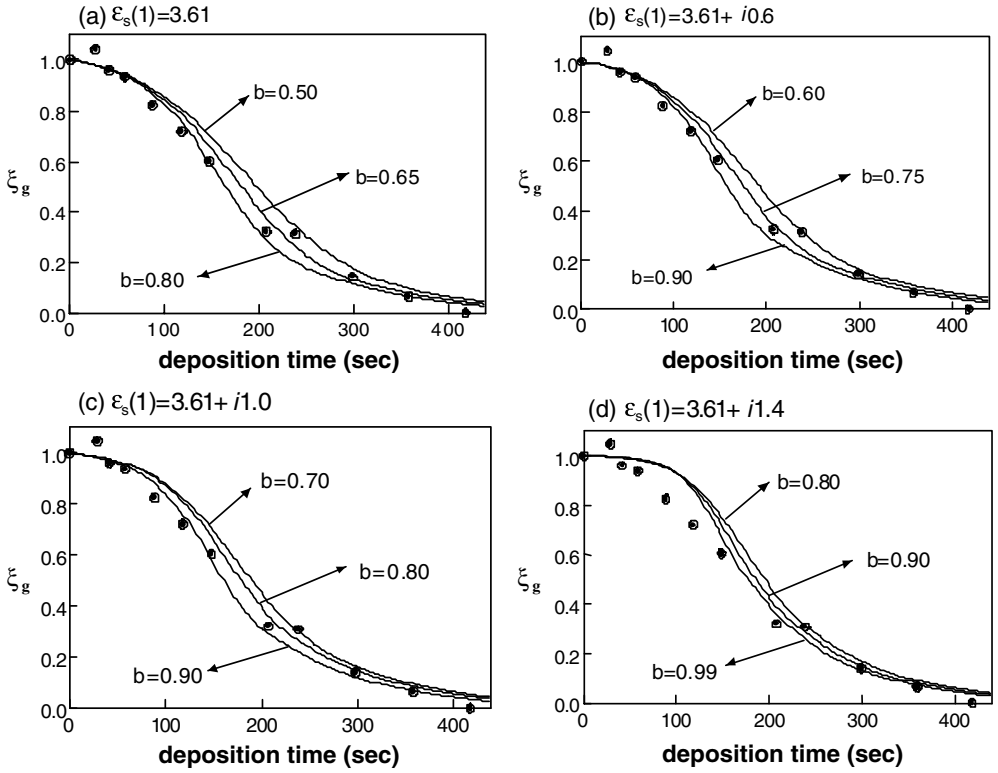

Figure 3. (a)–(d) Measured and simulated variation of the dipole scattering from C_{60}-covered graphite substrate. (●) Experimental data, while the curves are fitted results using different values of the step-crossing parameter b, as indicated. The four panels represent different values for $\varepsilon_s(1)$ shown.

4. Results

The simulated results are processed in the same manner as the experimental data in [7], where a coefficient analogous to the experimental substrate scattering-strength, ξ_g, is defined by normalizing the scattered signal to an elastic signal at each coverage and scaling it to unity for the bare graphite. In the present simulation, ξ_g is generated by using the following expression:

$$\xi_g = \frac{\alpha_{\text{total}}(t)}{I_0(t)} \frac{I_0(0)}{\alpha_{\text{total}}(0)}, \tag{6}$$

where $I_0(t)$ is the elastic scattering intensity described in [5] and t is the C_{60} deposition time. Figures 3(a)–(d) demonstrate the fits to obtain the experimental value for ξ_g. Since $\frac{|R_{C_{60}}|^2}{|R_g|^2}$ has been determined to be 0.14 [5], the fits are parameterized only by b, the probability of crossing a descending step, and $\varepsilon_s(1)$, the dielectric function of the first layer. Figure 3(a) shows a fit with $\varepsilon_s(1) = 3.61$, the same value as that for C_{60} layers above the first layer, i.e. we have assumed that it is not affected by the presence of the interface. The simulation gives a broad value for b, 0.65 ± 0.15, suggesting that the sensitivity of the ξ_g to surface morphology is not as high as $\xi_{C_{60}}$ (see [5]). This feature can be understood since ξ_g describes dipole scattering which, unlike impact scattering, occurs a few tens of angströms above the surface. However, we noted that a slightly smaller b value is obtained, compared to $b = 0.88 \pm 0.10$ obtained in our $\xi_{C_{60}}$ simulation.

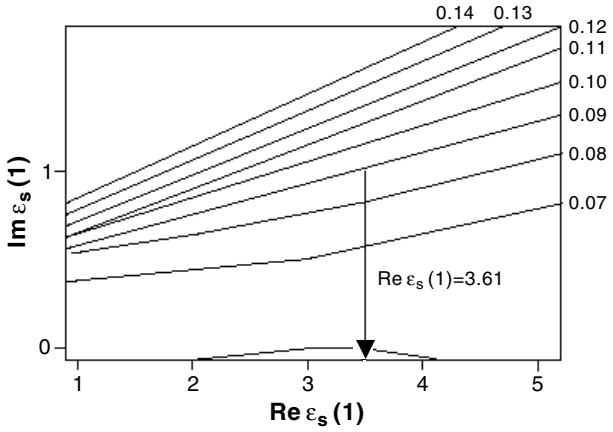

Figure 4. Contour map of the loss-function value for monolayer C_{60} on graphite in terms of its imaginary part, Im $\varepsilon_s(1)$, and its real part, Re $\varepsilon_s(1)$. The values of the contour are indicated. It is found that the value of the loss function should be smaller than 0.09 to obtain a qualified fit (see text). The arrow points out where $\varepsilon_s(1) = 3.61$.

We now take into account the interfacial effects by focusing on the first C_{60} overlayer on graphite, that is $\varepsilon_s(1)$. Adding an imaginary part to $\varepsilon_s(1)$ is found to effectively enhance the loss function (see figure 4, the contour of the loss function for monolayer C_{60} on graphite in terms of the real part and imaginary part of $\varepsilon_s(1)$). Figures 3(b)–(d) show fits by using $\varepsilon_s(1)$ containing an imaginary part. The role of the imaginary part in the fits is significant. By increasing slightly the imaginary part, the values of b are driven from 0.65 ± 0.15 to 0.80 ± 0.10, as shown in figures 3(a)–(c). Figure 3(d) shows an upper limit for the imaginary part, which has introduced a drastic deviation in the low deposition region.

Different values of the imaginary part show different degrees of enhancement in the cross section of the inelastic dipole scattering. It is worth checking how changes in $\varepsilon_s(1)$ vary the loss function for the graphite covered by one C_{60} layer. Figure 4 is a contour diagram of the loss function for monolayer C_{60} on graphite, in terms of the real part and imaginary part of $\varepsilon_s(1)$. Adding i1.4, for its effect in ξ_g simulation, see figure 3(d), has increased the value of the loss function from 0.07 to 0.11, which enhanced the cross section by 59%. On the other hand, the contour diagram also shows that the loss function is insensitive to the real part, so variation in the real part does not change the fits effectively.

To verify the above result, we combine signals from both impact scattering and dipole scattering to construct a series of EELS spectra to fit directly to the experimental data. The fitted parameters determined above and in our previous studies [5] are used to calculate the EELS spectra from 1 to 2.5 eV. The process is also a stringent test for the analysis since previously the fitted parameters were obtained at only one electron energy-loss value of 1 eV. The reconstructed spectra are given by

$$f_{re}(\Delta E, t) = \frac{f_g(1\text{ eV})}{\alpha_{total}(1\text{ eV}, 0)}\alpha_{total}(\Delta E, t) + \frac{f^s_{C_{60}}(\Delta E)}{I(420s)}I(t) \tag{7}$$

where $\alpha_{total}(\Delta E, t)$ and $I(t)$ are the cross section functions for dipole scattering and impact scattering; $f_g(1\text{ eV})$ is the intensity of the 1 eV loss point of the pure graphite spectrum, and $f^s_{C_{60}}(\Delta E)$ is the best-fit function for $f_{C_{60}}(\Delta E)$ which is the spectra from thick C_{60} films [5]. The two terms in equation (7) represent the features of the graphite intraband transitions and C_{60} HOMO–LUMO transitions, respectively. Two factors in front of the cross section functions

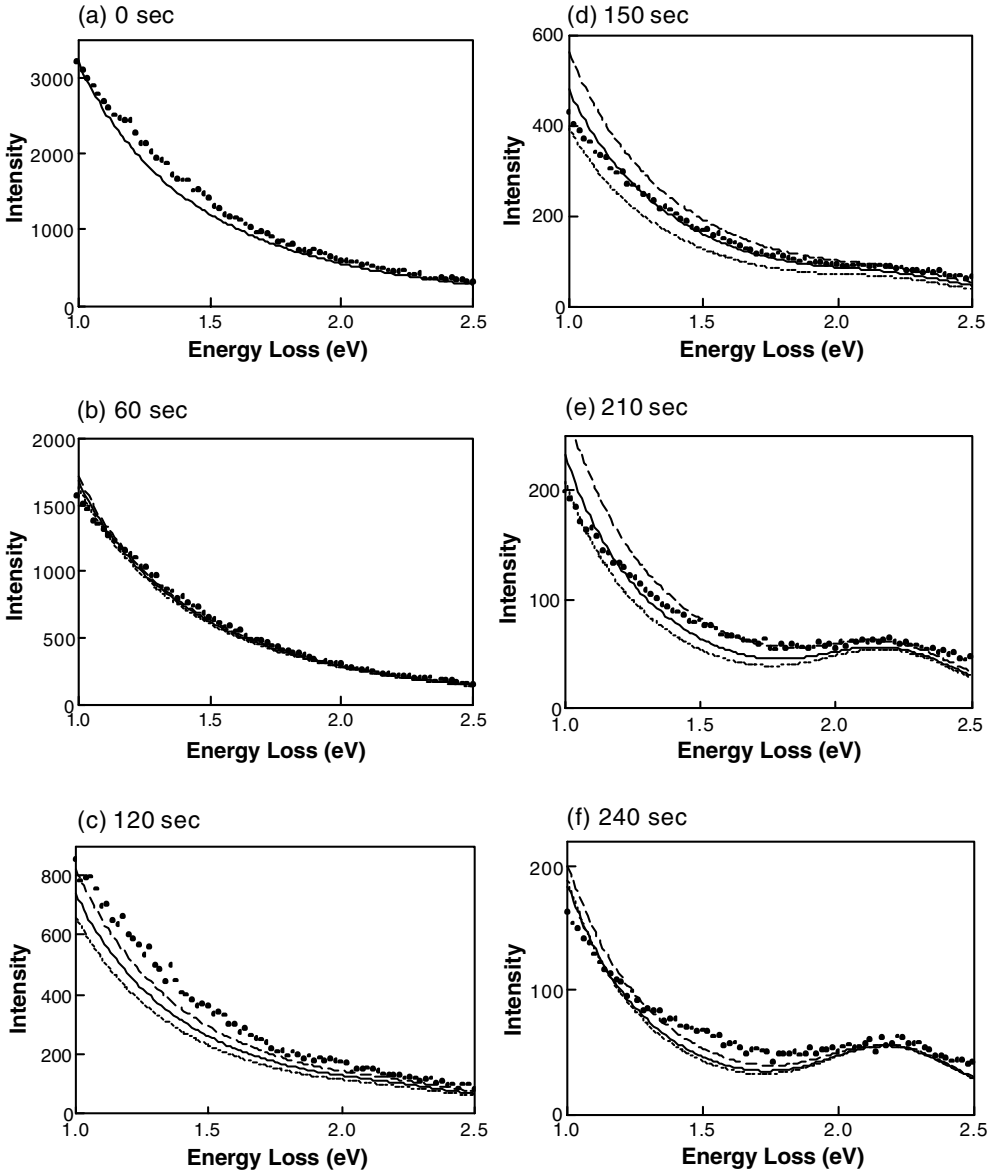

Figure 5. (a)–(f) Comparison of the experimental spectra with the reconstructed spectra at various stages in film growth. The filled dots are experimental data, the solid curves are the reconstructed spectra using $b = 0.80$, and the dashed curves and dotted curves denote those using $b = 0.70$ and 0.90, respectively. The six panels correspond to various deposition times, as indicated above the panels.

bring the reconstructed spectra to the two reference spectra, pure graphite and the thickest C_{60} film, at the two extremes, $t = 0$ and 420 s. Figure 5 is a series of comparisons of the best-fit curves with the experimental data. The good fit to the spectrum of pure graphite in figure 5(a) demonstrates the validity of the cross section function, equation (2), used to depict dipole scattering from graphite. The three simulated curves in figures 5(b)–(f) are generated by using

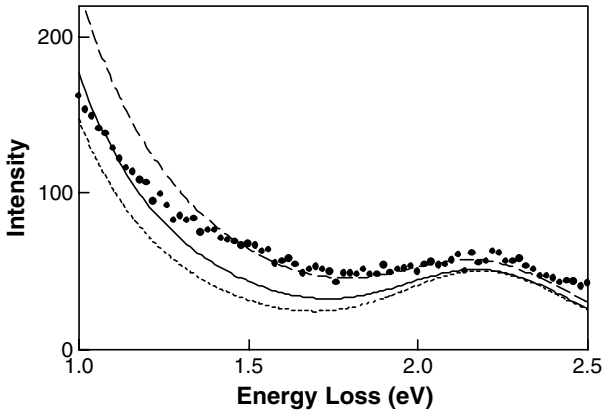

Figure 6. The reconstructed spectra of 240 s deposition using $\varepsilon_s(1) = 3.61$ and the corresponding step-crossing parameters ($b = 0.65 \pm 0.15$). The solid curve is the reconstructed spectrum obtained using $b = 0.65$, while the dashed and dotted curves are obtained using $b = 0.50$ and 0.80, respectively. The fit quality is worse than that shown in figure 5(f) for the same data but with different fitting parameters.

$b = 0.70$, 0.80, 0.90. For all curves, $\varepsilon_s(1) = 3.61 + i1.0$ is used for the dipole-scattering part. We assume that $\varepsilon_s(1)$ is not sensitive to the energy loss range. In both low deposition (60 s) and high deposition (240 s) cases, signals from either the pure graphite or thick C_{60} films dominate, and therefore the differences arising from various b become less evident, as shown. By using $\varepsilon_s(1)$ without the imaginary part and the corresponding lower step-crossing parameters ($b = 0.65$), one obtains a worse fit in the higher deposition region, as shown in figure 6.

5. Discussion and summary

Our simulation results demonstrate that the modification of the dielectric function in the interface leads to enhancement in the cross section of inelastic dipole scattering. Addition of the imaginary part of $\varepsilon_s(1)$ implies that new loss channels might be generated in the interface region, for example, electron redistribution or expansion of the electron–hole pair excitations in graphite. Other possibilities might involve the morphology of the submonolayer of C_{60}. It is interesting to note that a noticeable contribution of the imaginary part of the dielectric function in the optical gap region for single crystalline C_{60} is observed in polycrystalline C_{60} [22]. This was attributed to the large voids in the polycrystalline sample. This intriguing 'coincident' may support our argument that the interfacial interaction enhances the inelastic dipole scattering but quenches the inelastic impact scattering [5]. The dipole scattering occurs via the interactions of probe electrons with the electric field above the surface originating from the electronic excitation in surfaces. If the new electron loss channel originates from the electron redistribution, our results imply that they somehow reduce the capability of the C_{60} dielectric layer attenuating the electric field, thus reducing the probability of the substrate interacting with the probe electrons. In a separate study on C_{60} triplet exciton excitation, it was revealed that the excitation remained unchanged for monolayer C_{60} on graphite. Therefore, such possible redistribution of electrons in the interface would primarily be composed of the electrons of graphite surface states, and we speculate the graphite π electrons being highly involved.

In summary, by applying the two-layer dielectric model, we have simulated the strength of the inelastic dipole scattering from the graphite substrate during the growth of C_{60} thin films. The remarkably good quality of fit between the simulation spectra and the experimental spectra demonstrates the success of the employed combination of the dielectric model and the layered growth model in treating this system. It is found that, in order to better describe the electronic excitation for the monolayer C_{60}, the dielectric function has to include an imaginary part contribution, even in the optical band gap of the bulk single crystal C_{60}. The result implies that the C_{60}–graphite interfacial interaction may lead to additional electron loss channels. Further investigations on the optical properties of the coverage dependence of C_{60} on graphite by using, for example, spectroscopic ellipsometry measurements, could provide further insights to the mechanisms of the phenomena discussed in this paper.

References

[1] Ulbricht A, Moos G and Hertel T 2003 *Phys. Rev. Lett.* **90** 095501
[2] Noguch Y, Suzue Y and Iwamoto M 2003 *Curr. Appl. Phys.* **3** 397
[3] Rafii-Tabar H and Ghafoori-Tabrizi K 2001 *Prog. Surf. Sci.* **67** 217
[4] Kenny D J and Palmer R E 2000 *Surf. Sci.* **447** 126
[5] Luo M F, Li Z Y and Allison W 1999 *Surf. Sci.* **433–435** 590
[6] Li Z Y 1999 *Surf. Sci.* **441** 366
[7] Luo M F, Li Z Y and Allison W 1998 *Surf. Sci.* **402–404** 437
[8] Suto S, Kasuya A, Hu C W, Wawro A, Sakamoto K, Goto T and Nishina Y 1996 *Thin Solid Films* **281/282** 602
[9] Hunt M R C and Palmer R E 1996 *Surf. Rev. Lett.* **3** 937
[10] Richter H, Dereux A, Gilles J M, Guillaume C, Thiry P A, Lucas A A, Rozenberg R, Spote A, Hoffmann E, Girard C and Bunsenges B 1994 *Phys. Chem.* **98** 1329
[11] Lüthi R, Meyer E, Haefke H, Howald L, Gumannsbauer W and Guntherodt H J 1994 *Science* **266** 23
[12] Yu H, Yan J, Li Y, Yang W S, Gu Z and Wu Y 1993 *Surf. Sci.* **286** 116
[13] See, for example, Gravil P A, Devel M, Lambin Ph, Bouju X, Girard Ch and Lucas A A 1996 *Phys. Rev.* B **53** 1622
[14] See, for example, Goldoni A, Cepek C and Modesti S 1996 *Synth. Met.* **77** 189
Cepek C, Goldoni A, Modesti S, Negri F, Orlandi G and Zerbetto F 1996 *Chem. Phys. Lett.* **250** 537
[15] Palmer R E, Annett J F and Willis R F 1987 *Phys. Rev. Lett.* **58** 2490
[16] Ibach H and Mills D L 1982 *Electron Energy Loss Spectroscopy and Surface Vibrations* (New York: Academic)
[17] Danels J, Festenberg C V, Raether H and Zeppenfeld K 1970 *Springer Tracts in Modern Physics* vol 54 (Berlin: Springer)
[18] Ren S L, Wang Y, Rao A M, McRae E, Holden J M, Hager T, Wang K, Lee W T, Ni H F, Selegue J and Eklund P C 1991 *Appl. Phys. Lett.* **59** 2678
[19] Gravil P A, Devel M, Lambin Ph, Bouju X, Girard Ch and Lucas A A 1996 *Phys. Rev.* B **53** 1622
[20] Froitzheim H, Ibach H and Mills D L 1975 *Phys. Rev.* B **11** 4980
[21] Mills D L and Maradudin A A 1975 *Phys. Rev.* B **12** 2943
[22] Matsumoto K, Maeda H, Postava K, Takahashi K, Aoyama M, Yamaguchi T and Pistora J 2003 *Fullerences, Nanotubes Carbon Nanostruct.* **11** 15